Progress In Electromagnetics Research C, Vol. 87, 107–118, 2018

Gain and Bandwidth Enhancement of Circularly Polarized MSA Using PRS and AMC Layers

Shishir D. Jagtap[1, *], Rajiv K. Gupta[1], Nayana Chaskar[1], Shilpa Kharche[1], and Rajashree Thakare[2]

Abstract—In this paper, a circularly polarized (CP), high gain and wide bandwidth metal plated microstrip antenna (MSA) using partially reflecting surface (PRS) and artificial magnetic conductor (AMC) layers is proposed. The bandwidth of MSA is increased primarily, using AMC layers, and gain is increased by placing the antenna in a Fabry-Perot cavity (FPC) resonator. The two slotted AMCs are designed to resonate at two frequencies which electromagnetically couple to provide wide bandwidth. The FPC antenna with PRS and AMC layers provides higher gain, more impedance bandwidth, less gain variation and more miniaturization than the antenna without AMC layers. The proposed antenna provides $S_{11} < -10$ dB, axial ratio (AR) < 3 dB and 17.4 dBi peak gain with gain variation < 3 dB over 5.725 GHz to 6.4 GHz frequency band. Broadside radiation patterns have side lobe level (SLL) < -20 dB, cross polarization (CPL) < -16 dB and front to back (F/B) lobe ratio > 20 dB. The overall antenna dimensions are $2.83\lambda_0 \times 3.23\lambda_0 \times 0.49\lambda_0$, where λ_0 is the free space wavelength corresponding to the central frequency of 5.725–6.4 GHz. The proposed structure is fabricated, and the measured results agree with simulation ones.

1. INTRODUCTION

Presently, periodic structures, viz. artificial magnetic conductor (AMC), metasurface, frequency selective surface (FSS), partially reflecting surface (PRS), electromagnetic band gap (EBG) and high impedance surface (HIS) are used extensively to enhance the antenna performance [1–25]. An FPC resonator using a PRS is preferred over array antenna due to feed line losses and complexity in designing of the feed line network. Recently, multiple reflecting surfaces have been used to enhance the bandwidth and gain of the antenna. However, the state of art FPC antennas reported in [1–25] have either large size or low gain or narrow bandwidth and suffer from high SLL or high CPL. Therefore, to enhance gain and AR bandwidth of a CPMSA with low SLL and CPL and high F/B lobe ratio, a small size FPC antenna is designed using a slotted AMC layer, which is placed above the CPMSA, and the partial reflecting surface is loaded with another slotted AMC layer.

Gain enhancement of a left or right hand CPMSA over a narrow band using FPC is proposed in [1]. But the antenna has large size. The gain enhancement using FPC and a compact metasurface consisting of an array of square patches and annular slot rings is proposed in [2]. A compact wideband high gain CP antenna array using metasurface is proposed in [3]; however, it has high SLL and cross polar radiation. Wide-band antennas using a strip based metasurface [4] and a tapered metasurface [5] are proposed. To achieve wide bandwidth (BW), the concept of electromagnetic coupling of two resonating frequencies is used.

Received 22 July 2018, Accepted 13 September 2018, Scheduled 26 September 2018

* Corresponding author: Shishir Digamber Jagtap (shishir.jagtapd@gmail.com).

[1] Department of Electronics and Telecommunication, Terna Engineering College, Navi-Mumbai, India. [2] Department of Electronics and Telecommunication, Bharati Vidyapeeth College of Engineering, Navi-Mumbai, India.

The high gain and wide BW antennas using multilayer PRSs in FPC are proposed in [6, 7, 9–14, 17–19]. The PRS layers are designed to provide positive phase gradient to achieve high gain and wide BW. Homogeneous dielectric superstrate and periodic microstrip superstrate are used to increase the gain and BW of the antenna [6]. The analysis and design issues of different types of FSS are discussed in [7]. A multilayer dielectric cover is designed based on the Elliot synthesis method to enhance the gain and aperture efficiency of a waveguide slot array in [8]. The gain and BW enhancement of a patch antenna using two layers in FPC is proposed [9]. High gain wide-band CP antenna using two PRS layers is designed, but the antenna suffers from high SLL and CPL [10]. An EBG structure consisting of two complementary FSS layers is used to provide a positive reflection phase gradient and wide bandwidth [11]; however, it has significant SLL.

A high gain and wideband antenna using two [12] and three PRS layers [13] are reported. The antenna in [13] offers 20 dBi gain and bandwidth of 15%, but it has large dimensions. An aperture coupled broadband antenna using multilayer FSSs is designed in [14], but it has 4 dB gain variation over 4–5.4 GHz and high SLL and F/B lobe ratio < 10 dB. The high gain CPMSA using HIS in FPC is proposed in [15]. The directivity enhancement using FSS, EBG and metamaterial in FPC is proposed in [16]. A high gain and wideband FPC antenna using theory of tightly coupled antenna is proposed in [17]. The effect of various superstrate layers is analyzed using their reflection phase and magnitude response to reduce gain variations over a wide frequency band in [18]. A wide-band antenna using electrically thin superstrate and FPC is proposed in [19]. A reconfigurable FPC antenna with tunable HIS is designed to achieve beam steering in [20]. However, the proposed antenna has large aperture, high SLL and high gain variation as a function of scan angle. A high gain, reconfigurable dual band FPC antenna is proposed in [21].

A low profile, high gain wide band CP antenna with low radar cross-section area is designed by using three types of AMCs and metasurface [22]. The gain and BW enhancement of linearly polarized (LP) MSA using FSS cover and HIS in FPC is proposed in [23]. The three layers are combined to provide a stable reflection phase and flat gain bandwidth response. A tri-band antenna using two FSS layers in FPC is proposed [24]. These FSS layers can be adjusted to achieve either broadband or multiband antenna. A low profile, wideband, array antenna placed between reactive impedance surface (RIS) and PRS layers is reported in [25]. However, all these antennas either have large dimensions or provide low gain. Beside this, the antennas also have high SLL and cross polarization or narrow bandwidth than the proposed antenna.

In this paper, a novel, high gain wide band circularly polarized (CP) FPC antenna is proposed which offers SLL < 20 dB, CPL < -16 dB and F/B lobe ratio > 20 dB. The antenna operates over 5.725 GHz to 6.4 GHz, frequency band. The novelty of the structure is that, the slotted AMC layer above the CPMSA and the partial reflecting surface loaded with another slotted AMC layer in FPC, provide more AR bandwidth, less gain variation and more miniaturization of antenna.

2. ANTENNA GEOMETRY

The antenna geometry is shown in Fig. 1. The side view is shown in Fig. 1(a) while the top views of MSA, PRS-1, AMC-1 and AMC-2 are shown in Fig. 1(b) to Fig. 1(e) respectively. The gain and BW enhancement of a FPC antenna is achieved by placing a modified AMC-1 layer above the CPMSA and loading PRS-1 with AMC-2 which acts as PRS of FPC. MSA is suspended in air at 2 mm from the ground plane. The two, 1.59 mm thick, FR4 superstrate layers having dielectric constant and loss tangent of 4.4 and 0.02 respectively, are placed at 1 mm and 21.1 mm above the metal plated MSA. The AMC-1 is designed on one side of the lower superstrate, while, PRS-1 and AMC-2 are designed on upper superstrate as shown in Fig. 1. The AMC surfaces are designed by using an array of square patches of side 4 mm with inter-element spacing of 1 mm. The antenna structure is fed through a 50 Ω coaxial probe. The structures are simulated using method of moment based IE3D simulator.

3. DESIGN THEORY OF AMC SURFACES

The lower AMC surface is designed to resonate at higher frequency, and the upper AMC surface is designed to resonate at lower frequency which couples electromagnetically to provide wide ARBW.

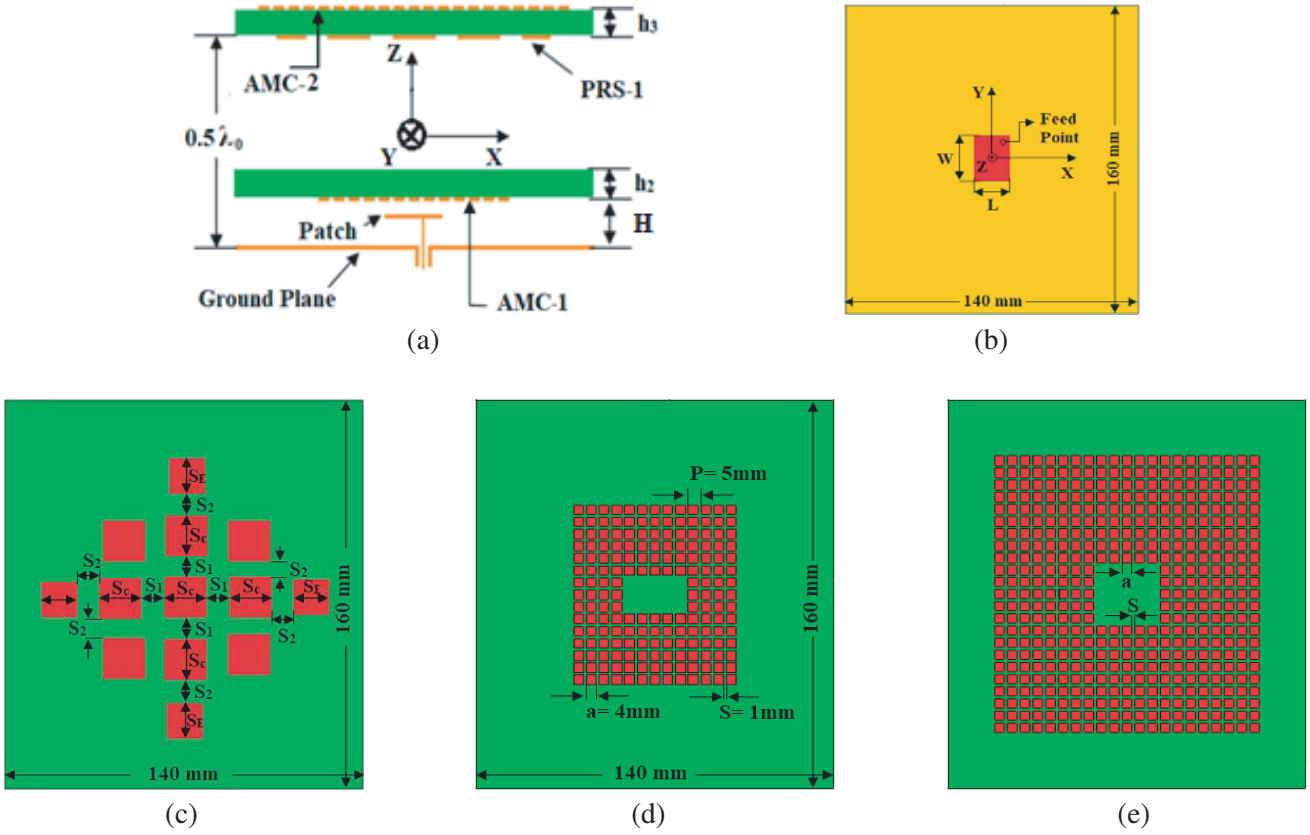

Figure 1. Geometry of the proposed antenna ($L = 16.2\,\text{mm}$, $W = 21.2\,\text{mm}$, feed position $(x, y) = 5.9\,\text{mm}, 7\,\text{mm}$, $S_c = 13\,\text{mm}$, $S_E = 11\,\text{mm}$, $S_1 = 9\,\text{mm}$ and $S_2 = 8\,\text{mm}$). (a) Side view. (b) CPMSA with ground plane. (c) PRS-1. (d) AMC-1. (e) AMC-2.

The AMC is formed using an array of square patches with periodicity much smaller than wavelength ($\leq 0.1\lambda_0$). The effect of change of periodicity and patch size of unit cell and its height from ground plane on AMC resonant frequency corresponding to 0° reflection phase crossing and AMC bandwidth corresponding to ±90° phase variation is studied using ANSYS High Frequency Structure Simulator (HFSS).

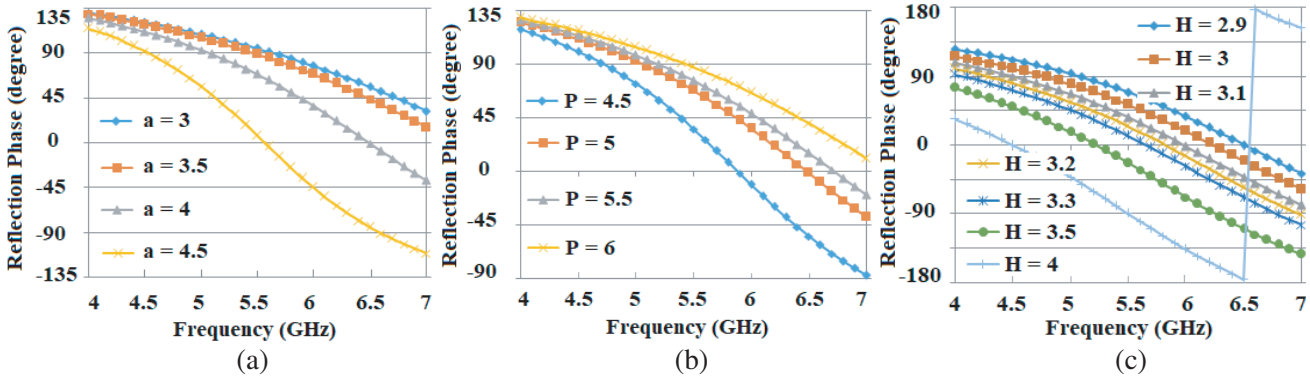

Figure 2. Reflection phase variation for different AMC square patch size, periodicity and height. (a) Square patch size. (b) Periodicity. (c) Height.

3.1. Effect of AMC Patch Size, Periodicity and Height

The effect of patch size and periodicity of the lower AMC is studied. The height of the AMC surface from the ground plane is fixed to 3 mm. For fixed periodicity ($P = 5$ mm), the resonant frequency decreases with increase in patch size 'a', and for fixed patch size ($a = 4$ mm), the resonant frequency increases with increase in periodicity 'P', as shown in Fig. 2(a) and Fig. 2(b) respectively [25]. Also, for $P = 5$ mm and $a = 4$ mm, the AMC resonance frequency decreases significantly with increase in the AMC surface height 'H' from the ground plane as shown in Fig. 2(c). The AMC surface with square patch dimension of side $a = 4$ mm, periodicity $P = 5$ mm and height $H = 3$ mm are selected since, it not only reduces the fabrication complexity but also resonates at 6.25 GHz and offers reflection phase variation of just $\pm 20°$ over 6 to 6.5 GHz, the upper band of the desired frequency band.

3.2. Effect of Number of Square Patches in a Unit Cell

The effect of number of patches in unit cell of AMC-1, on its reflection phase characteristics, is studied using HFSS. As the square patches in unit cell are increased from 1×1 to 3×3, AMC resonance frequency decreases slightly. However, increase in square patches in unit cell from 4×4 to 13×13 does not affect the AMC characteristics noticeably as shown in Figs. 3(a) and 3(b).

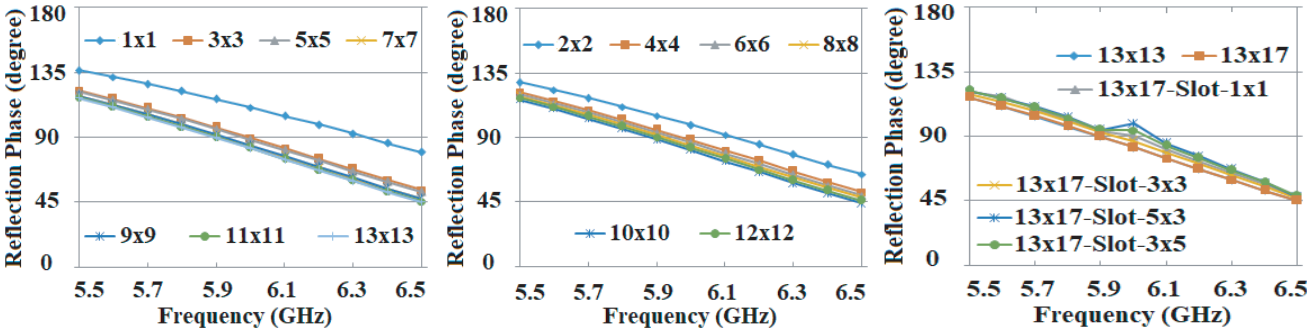

Figure 3. Reflection phase diagram of AMC with different cell size. (a) Odd patches. (b) Even patches. (c) With and without slot.

3.3. Effect of Removal of Square Patches in AMC

The effect of number of patches in unit cell of AMC-1 is studied to analyze the characteristics of a non-uniform slotted AMC surface. The main aim of introducing a slot in AMC surface is to increase ARBW of the antenna. The effect of slot size on reflection phase characteristics of AMC-1 and its effect on AMC resonance and BW are investigated in a unit cell with 13×17 square metallic patches. The slot size is varied from 1×1 to 5×3. The AMC resonance frequency increases with increase in the slot size, since, L and C of the AMC decrease with increase in slot size, as evident from the Fig. 3(c). The effect of change in slot size on antenna radiation characteristics using IE3D simulator is also studied and described in Section 5.

4. DESIGN THEORY OF PRS-1 AND AMC-2

The gain and ARBW of MSA with slotted AMC-1 are increased further by using FPC. The FPC is formed by placing a PRS-1 loaded with AMC-2, together acting as a PRS, nearly $0.5\lambda_0$ above the MSA. The PRS-1 is formed by printing square patch/patches of 0.5λ side spaced at nearly 1.0λ on the lower side, where λ is the wavelength in the dielectric medium, and AMC-2 is formed by fabricating an array of 4 mm square patches with periodicity 5 mm on the upper side of the FR4 superstrate as shown in Fig. 1(a). The unit cells of AMC-1, AMC-1 with AMC-2 and AMC-2 with PRS-1, are shown in Fig. 4(a) to Fig. 4(c), respectively. The AMC-2 is designed to resonate at about 5.85 GHz. PRS-1 is designed to

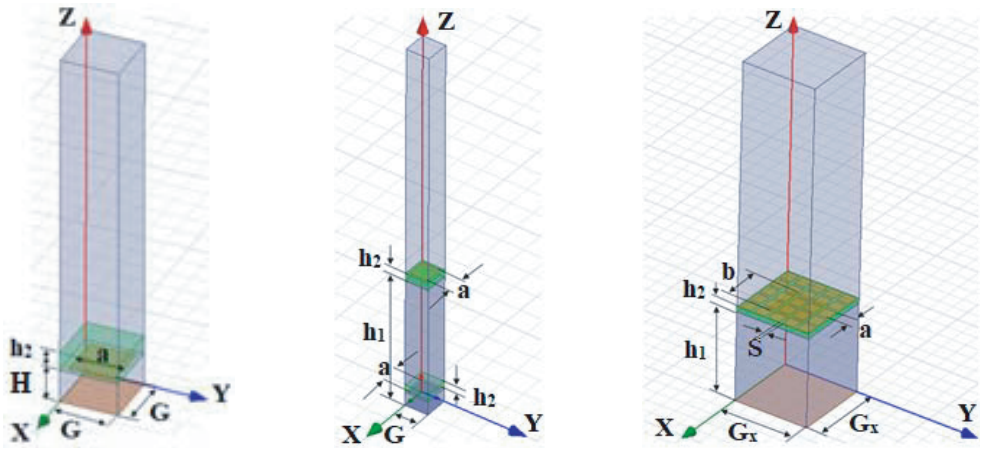

Figure 4. Unit cell of the AMC and PRS layers. (a) AMC-1. (b) AMC-1 and AMC-2. (c) PRS-1 and AMC-2. ($G = 5$, $H = 3$, $a = 4$, $h_1 = 22.7$, $h_2 = 1.59$, $G_x = 25$, $b = 13$, $S = 1$, all dimensions are in mm).

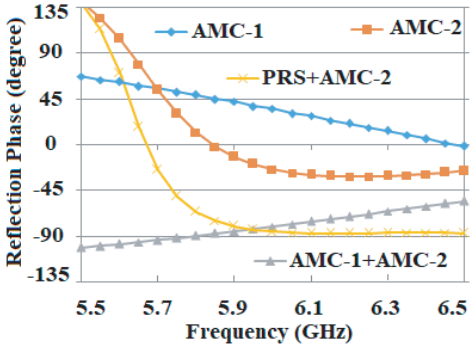

Figure 5. Reflection phase variation.

resonate at about 5.8 GHz. The AMC-2 with PRS-1 should have reflection phase variation within $\pm 90°$ over 5.725 to 6.4 GHz band.

The PRS-1 when being loaded with AMC-2 increases the inductive and the capacitive coupling between the two surfaces. AMC-2 with PRS-1 has higher L and C, and therefore, it resonates at lower frequency 5.67 GHz than 5.85 GHz, the resonant frequency of AMC-2 alone, as shown in Fig. 5. The PRS-1 has a square metallic patch of side 13 mm and inter-element spacing of about 25 mm. Therefore, unit cell with square ground plane of side 25 mm is selected, while AMC-2 has 5×5, 4 mm square patches with spacing of 1 mm, as shown in Fig. 4(c). Further, removal of a patch or an array of patches from AMC-2 surface also increases the resonant frequency and reflection phase and helps in increasing ARBW.

The optimized patch size and periodicity of AMC-1 and AMC-2 surface are 4 mm and 5 mm, respectively. The optimized heights of AMC-1 and AMC-2 surface are 3 mm and 24.29 mm from ground plane, respectively.

5. RESONANT CONDITION AND GAIN OF FPC ANTENNA

The reflection phase variations of AMC-1 and AMC-2 with PRS-1 are denoted by $\emptyset_1(f)$ and $\emptyset_2(f)$, respectively. The resonant condition of FPC having AMC and PRS surfaces is given by [23],

$$\frac{4\pi h_1}{c} f - \emptyset_1(f) - \emptyset_2(f) = 2N\pi \quad (N = 0, 1, 2...)$$

where c is the velocity of wave in free space, and N is the order of the resonant mode.

Assume $\theta(f) = \emptyset_1(f) + \emptyset_2(f)$ and $\varphi(f) = \frac{4\pi h_1}{c} f - 2N\pi$.

The intersection of $\theta(f)$ and $\varphi(f)$ curves corresponds to the resonant frequency of the antenna structure. The $\theta(f)$ and $\varphi(f)$ curves are plotted in Fig. 6(a). A correction of 12 degrees is added to $\theta(f)$ curve, due to slot in AMC-1 and AMC-2. The slot in AMC surface increases the reflection phase and resonant frequency. The corrected $\theta(f)$ and $\varphi(f)$ curves intersect at 5.9 GHz, which is close to 6.0625 GHz, the central frequency of operating band from 5.725 GHz to 6.4 GHz.

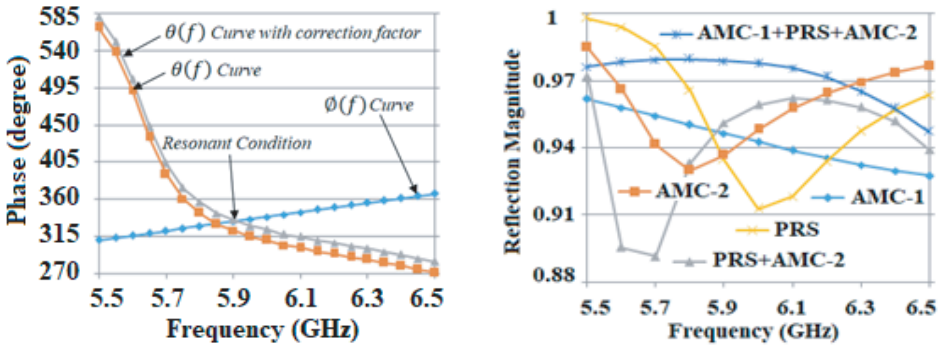

Figure 6. (a) Resonant conditions and (b) reflection magnitude.

The antenna, considered here, is an FPC antenna, whose gain depends on feed antenna and reflection coefficient of PRS. AMC-2 and PRS-1 together form PRS, and AMC-1 acts as another reflecting surface in FPC. FPC with a PRS causes multiple reflections and transmissions. High gain and directivity can be achieved if all these transmitted waves are in phase. Also, the gain of the FPC antenna is given by,

$$G = \frac{1+\rho}{1-\rho}$$

Here, ρ is the magnitude of reflection coefficient of PRS.

As shown in Fig. 6(b), the reflection magnitude of individual PRS-1 or AMC layers has lower values and more variations than the combined PRS and AMC-1 layers. Therefore, the proposed antenna, with PRS and AMC layers together, offers high gain over wide band, as compared to antenna with PRS-1 alone.

6. SIMULATION RESULTS AND ANALYSIS

6.1. ARBW Enhancement of CPMSA Using Slotted AMC Layer

The aim is to design a high gain CP antenna to operate over 5.725 GHz to 6.4 GHz frequency band. Initially, a 21 mm × 23 mm metal plated CPMSA is designed at 6.15 GHz. The MSA is suspended in air at a height $h = 2$ mm from 0.5 mm thick, 60 mm × 70 mm copper metal ground plane and fed diagonally using a 50 Ω coaxial probe at $(x, y) = (3\,\text{mm}, 5\,\text{mm})$ to excite the orthogonal modes and generate circular polarization. The antenna provides 10.4 dBi peak gain and 160 MHz ARBW as shown in Fig. 7. To increase the ARBW, initially, a uniform AMC-1, formed by a 13 × 15 array of 4 mm square patches with spacing of 1 mm, is printed on bottom side of an FR4 superstrate and placed 1 mm above the CPMSA. The AMC-1 is equivalent to L-C circuit and has its own resonant frequency, which, in this case, is lower than MSA resonant frequency. The dimensions of MSA are optimized to 17 mm × 20 mm so that AMC-1 and MSA resonate at different but nearby frequencies and couple electromagnetically to provide wide impedance BW as shown in Fig. 8. This antenna provides 9.3 dBi peak gain and 290 MHz ARBW. The ARBW is further improved, by modifying the uniform AMC-1. 5 × 3 central square patches in the uniform AMC-1 are removed to form a rectangular slot of 25 mm × 15 mm in the uniform AMC-1

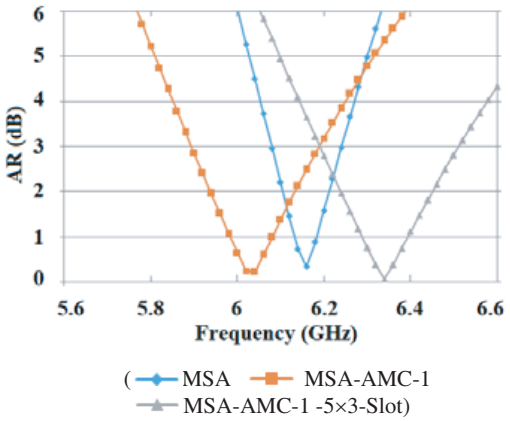

Figure 7. Axial ratio vs. frequency.

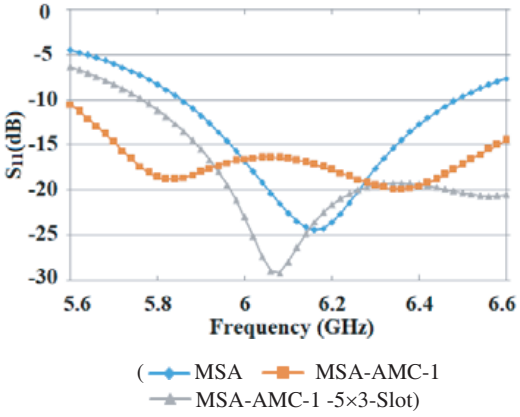

Figure 8. S_{11} vs. frequency.

as shown in Fig. 1. The length of the slot is more than width, in contrary to metal plated MSA. The slot having length/width ratio > 1 in AMC-1 and the MSA having length/width < 1 resonate at two different but nearby frequencies and electromagnetically couple to provide wide ARBW. The modified AMC-1 resonates at higher frequency than uniform AMC-1, since, removing patches in AMC-1, reduces L and C, which is evident from Fig. 8. This antenna with modified AMC-1 provides 9.3 dBi peak gain and ARBW of 320 MHz.

6.2. Gain and ARBW Enhancement Using PRS-1 Loaded with Slotted AMC Layer

Now, to increase the gain of the antenna, the CPMSA with modified AMC-1 is placed in FPC. The PRS-1 layer is placed at about $0.5\lambda_0$ height, from the ground plane. The PRS-1 is formed by printing an array of square patches on the bottom side of FR4 superstrate as shown in Fig. 1(c). Initially, a single square patch of side 13 mm, which is about 0.5λ long, where λ is the wavelength in dielectric corresponding to 5.8 GHz, is printed on PRS-1. This single parasitic patch on the PRS-1 also acts as a space fed patch antenna. Metallic patch increases the reflection coefficient of PRS and therefore increases the gain of the antenna. The optimized structure provides, 13.1 dBi peak gain, CPL < -13.5 dB, SLL < -20 dB and F/B > 17 dB. Impedance BW > 1 GHz and 660 MHz (5.84 GHz to 6.5 GHz) ARBW is achieved. The gain and ARBW of this antenna are enhanced by 3.8 dB and 340 MHz, respectively, as compared to the antenna without PRS-1 layer.

Now, an AMC-2, as shown in Fig. 1(e), is printed on the upper side of an FR4 superstrate, and this antenna structure is termed as 'Ant1'. The AMC-2 reduces phase variation of the fields over wide frequency band, giving rise to wide BW. The addition of AMC-2 not only increases the ARBW but

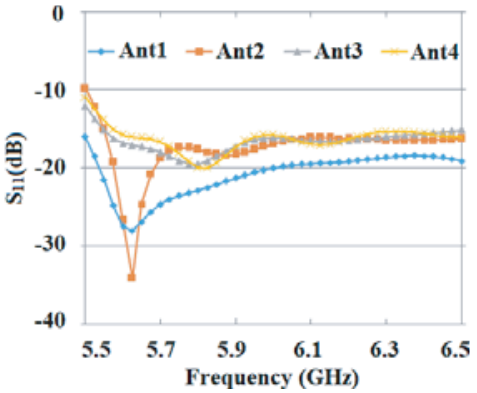

Figure 9. S_{11} vs. frequency.

also increases reflection coefficient of PRS layer and hence, increases the gain of the antenna. The optimized 'Ant1' provides 14.4 dBi peak gain, CPL < -15.8 dB, SLL < -20 dB and F/B > 16 dB. 840 MHz (5.66 GHz to 6.5 GHz) ARBW is achieved which corresponds to 14.48%. The gain and ARBW are improved by 1.21 dB and 350 MHz, respectively as compared to antenna without AMC-2 layer. The gain variation < 2 dB is achieved over 5.5 to 6.5 GHz. The 'Ant1' also offers less CPL and SLL than the antenna without AMC-2 layer.

Thereafter, in 'Ant2', 2×2 array of square patches of side 13 mm with spacing of 9 mm is placed at PRS-1. These 2×2 patches act as a space fed array antenna. The size and periodicity of PRS-1 patches are larger than AMC-1 and AMC-2. Similarly, 'Ant3' with 3×3 array and 'Ant4' in which a patch is placed on all four sides of 3×3 array, along X and Y axes on the superstrate, are designed and optimized. The antenna ground plane size is increased, nearly by $0.5\lambda_0$ each time, with increase in array size from 1×1 to 3×3 of PRS, so that F/B ratio > 20 dB. The S_{11} variations of 'Ant1' to 'Ant4' are shown in Fig. 9. AR < 3 dB, over 5.725 to 6.4 GHz frequency band, is achieved in all the antennas as shown in Fig. 10(a).

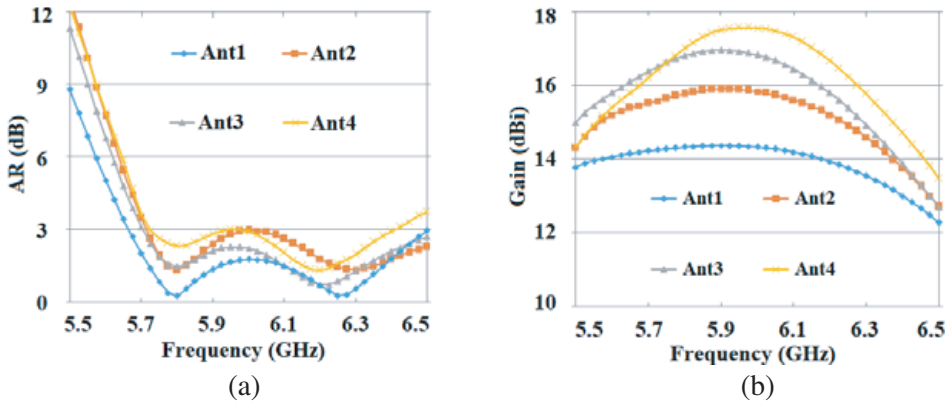

Figure 10. (a) Axial ratio and (b) gain variation vs. frequency.

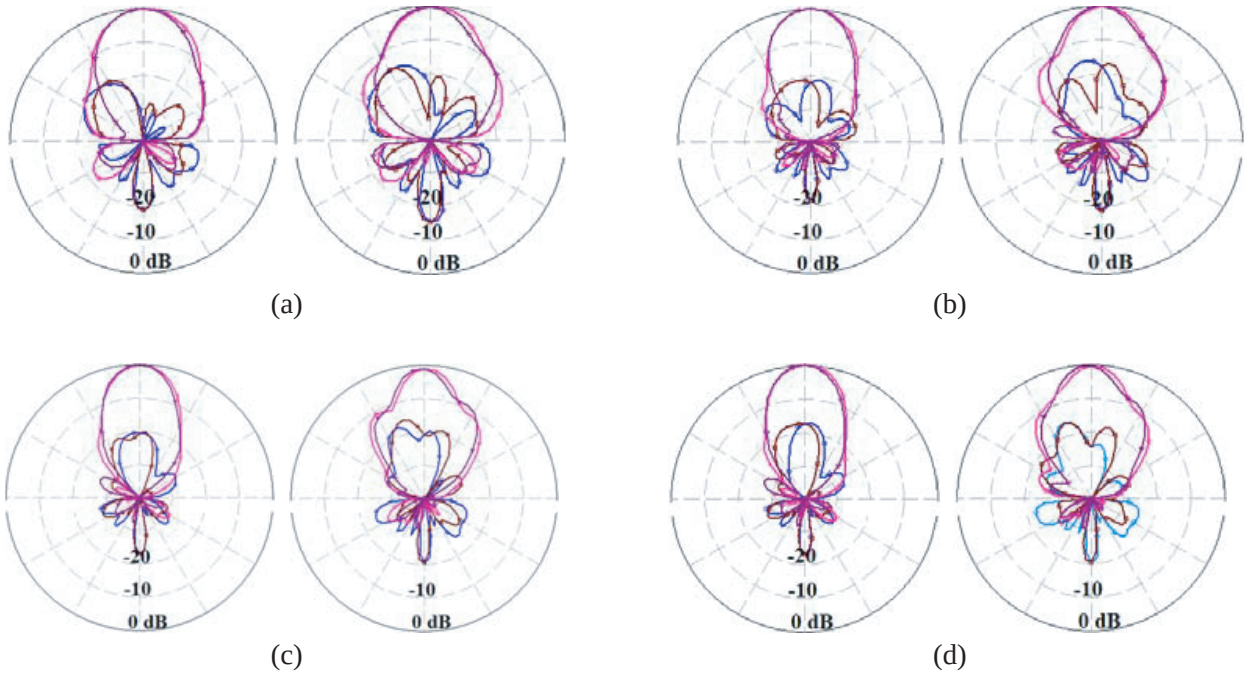

Figure 11. Radiation patterns at 5.8 GHz and 6.15 GHz. (a) Ant1. (b) Ant2. (c) Ant3. (d) Ant4.

Gain of the antenna increases from 14.4 dB to 17 dBi with increase in array size of parasitic patches (PPs) from 1×1 to 3×3 as shown in Fig. 10(b). However, this increases gain variation over wide frequency band, thereby reducing 3 dB gain BW. The PPs are fed from the radiating field of MSA. The dimensions of PPs are decreased progressively as its distance from the MSA increases to compensate the phase delay in feed. The spacing between the patches is also decreased to enhance the reflection of PRS and the gain of the antenna and to decrease the gain variation. The resonance frequency of the structure increases with decrease in dimension and spacing of patches and therefore the gain at higher frequency increases which decreases the gain variation. 'Ant4' is designed to increase the gain further to 17.6 dBi by placing a patch on all four sides of 3×3 array along X and Y axes on the superstrate. The broadside radiation patterns of 'Ant1' to 'Ant4'at 5.8 GHz and 6.15 GHz are shown in Fig. 11. Radiation patterns are symmetrical in broadside direction. The radiation parameters for Ant1 to Ant4 structures at 5.8 GHz and 6.15 GHz are listed in Table 1.

Table 1. Radiation parameters of structures.

Ant	Peak Gain (dBi)	3 dB Gain BW (MHz)	ARBW (MHz)	Global BW (MHz)	5.8 GHz (dB)			6.15 GHz (dB)			Size (mm^3/λ_0^3) $\lambda_0 \approx$ 49.5 mm at 6.0625 GHz
					SLL	CPL	F/B	SLL	CPL	F/B	
Ant1	14.4	>1000	840	840	-22.2	-18.5	19.1	-20.2	-15.8	15.7	90×110×29.59 1.82×2.2×0.6
Ant2	15.9	>990	802	≈ 800	-20.0	-21.2	22.5	-26.4	-16.3	19.5	120×140×28.59 2.42×2.83×0.57
Ant3	16.9	>880	640	640	-27.6	-19.8	23.4	-23.4	-16.6	21.2	140×160×28.29 2.83×3.23×0.57
Ant4	17.4	>890	702	702.5	-26.9	-17.3	23.5	-22.7	-16.1	20.8	140×160×24.29 2.83×3.23×0.49

7. FABRICATION AND MEASURED RESULTS

The fabricated 'Ant4' structure is shown in Fig. 12. S_{11} is measured by using 9916A Agilent network analyzer, and gain and radiation patterns of the antenna are measured using standard horn antenna. The simulated and measured S_{11} and gains are shown in Fig. 13(a), while the simulated and measured axial ratios are shown in Fig. 13(b). The measured results closely match the simulation ones. The small variation in simulated and measured results may be attributed to fabrication errors. The measured radiation patterns at 5.8 GHz and 6.15 GHz are shown in Fig. 14. Broadside radiation patterns are

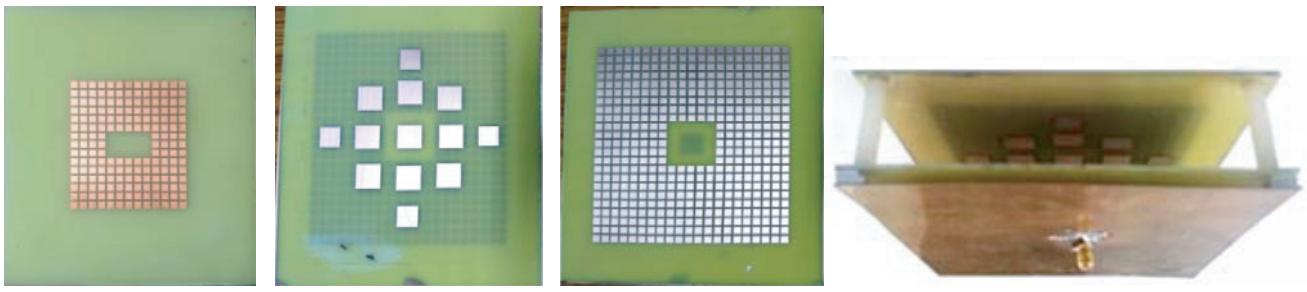

(a) (b) (c) (d)

Figure 12. Photograph of 'Ant4' prototype. (a) Top view of AMC-1. (b) Top view of PRS. (c) Top view of AMC-2. (d) 3D view.

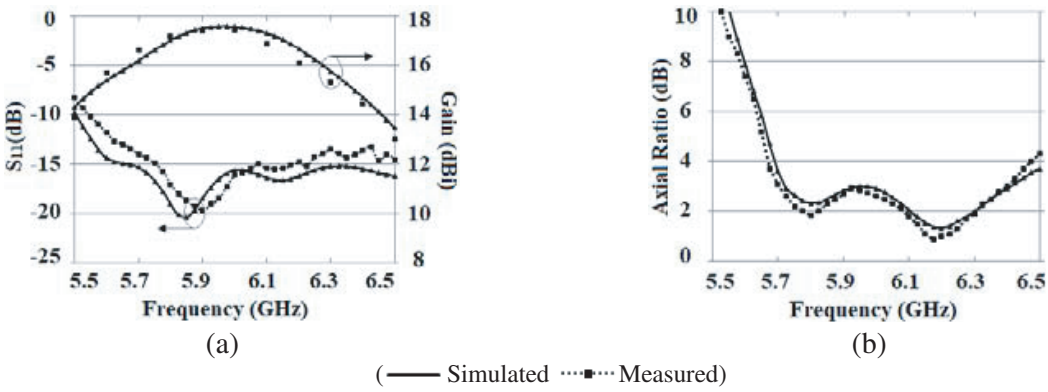

Figure 13. (a) Gain and S_{11} vs. frequency. (b) Axial ratio vs. frequency of 'Ant4'.

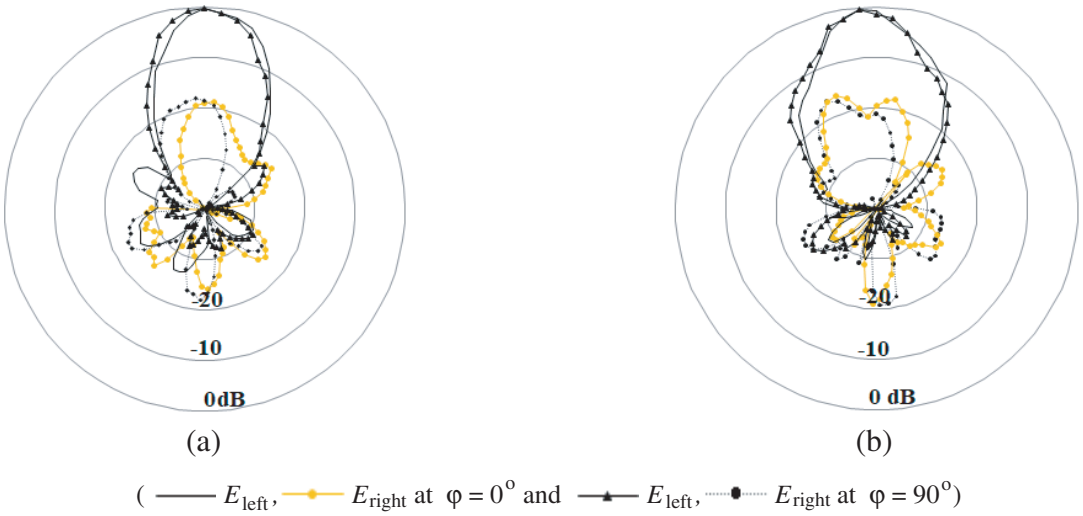

Figure 14. Radiation patterns of 'Ant4'. (a) 5.8 GHz. (b) 6.15 GHz.

obtained with little variation over the entire frequency band. The radiation patterns of the proposed antenna structure have SLL < -20 dB, cross polarization < -16 dB and F/B lobe ratio > 20 dB.

8. COMPARISON OF THE PROPOSED ANTENNA WITH SIMILAR EXISTING ANTENNAS

The comparison of the proposed antenna with existing state of art linearly and circularly polarized antenna structures using FPC is listed in Table 2. The gains of the antennas in [1, 2, 18, 20] are comparable to the proposed antenna; however, the antennas proposed in [1, 20] have larger dimensions. Antennas reported in [2, 18, 20] have higher SLL. The BW of the antennas presented in [9–11 and 14] is significantly more than the proposed antenna; however, these structures have less gain and high SLL. The BW of the antenna stated in [12] is more, but, the proposed antenna has significantly larger gain than the one reported in [12]. The size of the antennas presented in [13, 15 and 23] is larger than the proposed antenna. Antennas reported in [13 and 23] are LP antennas and have higher SLL, while the one presented in [15] offers only 3% BW.

Table 2. Comparison of the proposed antenna with reference antennas.

Ref.	Pol.	Gain dBi	SLL (dB)	CPL (dB)	F/B (dB)	Global BW (%)	Size of the Antenna $\lambda_0^3/(\text{mm}^3)$
[1]	CP	17.3	−25	−26	21	2.6	$5\lambda_0 \times 5\lambda_0 \times 0.5\lambda_0$
[2]	LP	16.35	−7	NR	16	NR(< 2)	$2.21\lambda_0 \times 2.21\lambda_0 \times 0.578\lambda_0$
[9]	LP	15	−11	−25	17	25.8	$2.4\lambda_0 \times 2.4\lambda_0 \times 1.4\lambda_0$
[10]	CP	14.7	−12	−12	15	28.3	$2.77\lambda_0 \times 2.77\lambda_0 \times 0.69\lambda_0$
[11]	LP	13.8	−12	−21	13	28	$2.4\lambda_0 \times 2.4\lambda_0 \times 0.55\lambda_0$
[12]	LP	10.5	NR	−15	NR	14.7	$2\lambda_0 \times 2\lambda_0 \times 0.77\lambda_0$
[13]	LP	20	-8	NR	NR	15	$3.87\lambda_0 \times 3.87\lambda_0 \times 1.77\lambda_0$
[14]	LP	14.2	−9	NR	14	30	$1.6\lambda_0 \times 1.6\lambda_0 \times 0.84\lambda_0$
[15]	CP	19.1	−20	−17.5	NR	3	$6.88\lambda_0 \times 6.88\lambda_0 \times 0.524\lambda_0$
[18]	LP	16	−9.5	NR	13	23	$2.75\lambda_0 \times 2.75\lambda_0 \times 0.56\lambda_0$
[20]	LP	16.1	−5	NR	NR	NR	$5.4\lambda_0 \times 5.4\lambda_0 \times 0.5\lambda_0$
[23]	LP	19.1	−13	−22	20	14.1	$2.94\lambda_0 \times 3.43\lambda_0 \times 0.59\lambda_0$
Proposed	CP	17.4	−20	−16	20	11.6	$2.83\lambda_0 \times 3.23\lambda_0 \times 0.49\lambda_0$

9. CONCLUSION

A high gain and wide band circularly polarized antenna using PRS and modified AMC layers is designed to operate over 5.725 GHz to 6.4 GHz frequency band, which covers 5.725 GHz to 5.875 GHz, ISM frequency band and 5.9 GHz to 6.4 GHz, satellite C band. The proposed antenna offers a peak gain of 17.4 dBi and bandwidth of 11.6%.

REFERENCES

1. Vaidya, A. R., R. K. Gupta, S. K. Mishra, and J. Mukherjee, "Right-hand/left-hand circularly polarized high-gain antennas using partially reflective surfaces," *IEEE Antennas and Wireless Propagation Letters*, Vol. 13, 431–434, 2014.
2. Singh, A. K., M. P. Abegaonkar, and S. K. Koul, "High-gain and high-aperture-efficiency cavity resonator antenna using metamaterial superstrate," *IEEE Antennas and Wireless Propagation Letters*, Vol. 16, 2388–2391, 2017.
3. Ta, S. X. and I. Park, "Compact wideband circularly polarized patch antenna array using metasurface," *IEEE Antennas and Wireless Propagation Letters*, Vol. 16, 1932–1936, Mar. 2017.
4. Martinis, M., L. Bernard, K. Mahdjoubi, R. Sauleau, and S. Collardey, "Wideband antenna in cavity based on metasurfaces," *IEEE Antennas and Wireless Propagation Letters*, Vol. 15, 1053–1056, 2016.
5. Feng, G., L. Chen, X. Xue, and X. Shi, "Broadband surface-wave antenna with a novelnonuniform tapered metasurface," *IEEE Antennas and Wireless Propagation Letters*, Vol. 16, 2902–2905, 2017.
6. Chen, X., Z. Luo, P. Feng, and K. Huang, "Effective reflective characteristics of superstrates and their effects on the resonant cavity antenna," *IEEE Transactions on Antennas and Propagation*, Vol. 63, No. 4, 1572–1580, Apr. 2015.
7. Narayan, S. and R. M. Jha, "Electromagnetic techniques and design strategies for FSS structure applications," *IEEE Antennas and Propagation Magazine*, 135–143, Oct. 2015.
8. Montisci, G., Z. S. Jin, M. C. Li, et al., "Design of multilayer dielectric cover to enhance gain and efficiency of slot arrays," *International Journal of Antennas and Propagation*, Vol. 2013, 6 pages, Article ID 917676, 2013.

9. Wang, N., J. Li, G. Wei, L. Talbi, Q. Zeng, and J. Xu, "Wideband Fabry-Perot resonator antenna with two layers of dielectric superstrates," *IEEE Antennas and Wireless Propagation Letters*, Vol. 14, 229–232, 2015.
10. Qin, F., S. Gao, G. Wei, Q. Luo, C.-X. Mao, C. Gu, J. Xu, and J. Li, "Wideband circularly polarized Fabry-Perot antenna," *IEEE Antennas and Propagation Magazine*, 127–135, Oct. 2015.
11. Wang, N., Q. Liu, C. Wu, L. Talbi, Q. Zeng, and J. Xu, "Wideband Fabry-Perot resonator antenna with two complementary FSS layers," *IEEE Transactions on Antennas and Propagation*, Vol. 62, No. 5, 2463–2471, May 2014.
12. Vaid, S. and A. Mittal, "Wideband orthogonally polarized resonant cavity antennawith dual layer Jerusalem cross partially reflective surface," *Progress In Electromagnetics Research C*, Vol. 72, 105–113, 2017.
13. Konstantinidis, K., A. P. Feresidis, and P. S. Hall, "Multilayer partially reflective surfaces for broadband Fabry-Perot cavity antennas," *IEEE Transactions on Antennas and Propagation*, Vol. 62, No. 7, 3474–3481, Jul. 2014.
14. Chacko, B. P., G. Augustin, and T. A. Denidni, "FPC antennas, C-band, point to point communication," *IEEE Antennas and Propagation Magazine*, Vol. 62, No. 1, 19–26, Jan. 2014.
15. Orr, R., G. Goussetis, and V. Fusco, "Design method for circularly polarized Fabry Perot cavity antennas," *IEEE Transactions on Antennas and Propagation*, Vol. 62, No. 7, 3474–3481, 2014.
16. Liu, H., S. Lei, X. Shi, and L. Li, "Study of antenna superstrates using metamaterials for directivity enhancement based on Fabry Perot resonant cavity," *International Journal of Antennas and Propagation*, Vol. 2013, 1–10, Article-ID 209741, Hindwai Publishing Corporation, 2013.
17. Xu, Y., R. Lian, Z. Wang, and Y.-Z. Yin, "Wideband Fabry-Perot resonator antenna with single-layer partially reflective surface," *Progress In Electromagnetics Research Letters*, Vol. 65, 37–41, 2017.
18. Ji, L.-Y., P.-Y. Qin, and Y. J. Guo, "Wideband Fabry-Perot cavity antenna with a shaped ground plane," *IEEE Access*, Vol. 6, 2291–2297, 2018.
19. Wang, N., L. Talbi, Q. Zeng, and J. Xu, "Wideband Fabry-Perot resonator antenna withelectrically thin dielectric superstrates," *IEEE Access*, Vol. 6, 14966–14973, 2018.
20. Guzman-Quiros, R., A. R. Weily, J. L. Gomez-Tornero, and Y. J. Guo, "A Fabry-Perot antenna with two-dimensional electronic beam scanning," *IEEE Antennas and Wireless Propagation Letters*, Vol. 14, 1014–1017, 2015.
21. Xie, P. and G.-M. Wang, "Design of a frequency reconfigurable Fabry Perot cavity antenna with single layer partially reflecting surface," *Progress In Electromagnetics Research Letters*, Vol. 70, 115–121, 2017.
22. Jia, Y., Y. Liu, S. Gong, W. Zhang, and G. Liao, "A low RCS and high gain circularly polarized antenna with a low profile," *IEEE Antennas and Wireless Propagation Letters*, Vol. 16, 2477–2480, 2017.
23. Wu, Z.-H. and W.-X. Zhang, "Broadband printed compound air-fed array antennas," *IEEE Antennas and Wireless Propagation Letters*, Vol. 9, 187–191, 2010.
24. Qin, F., S. Gao, Q. Luo, G. Wei, J. Xu, J. Li, C. Wu, C. Gu, and C. Mao, "A triband low-profile high-gain planar antenna using Fabry-Perot cavity," *IEEE Transactions on Antennas and Propagation*, Vol. 65, No. 5, 2683–2688, 2016.
25. Jagtap, S., A. Chaudhari, N. Chaskar, S. Kharche, and R. K. Gupta, "A wideband microstrip array design using RIS and PRS layers," *IEEE Antennas and Wireless Propagation Letters*, Vol. 17, 509–512, Mar. 2018.